

# TAPS: Connecting Certified and Adversarial Training

Yuhao Mao<sup>1</sup> Mark Niklas Müller<sup>1</sup> Marc Fischer<sup>1</sup> Martin Vechev<sup>1</sup>

## Abstract

Training certifiably robust neural networks remains a notoriously hard problem. On one side, adversarial training optimizes under-approximations of the worst-case loss, which leads to insufficient regularization for certification, while on the other, sound certified training methods optimize loose over-approximations, leading to over-regularization and poor (standard) accuracy. In this work we propose TAPS, an (un-sound) certified training method that combines IBP and PGD training to yield precise, although not necessarily sound, worst-case loss approximations, reducing over-regularization and increasing certified and standard accuracies. Empirically, TAPS achieves a new state-of-the-art in many settings, e.g., reaching a certified accuracy of 22% on TINYIMAGENET for  $\ell_\infty$ -perturbations with radius  $\epsilon = 1/255$ .

## 1. Introduction

Robustness to adversarial attacks, *i.e.*, small, imperceptible input perturbations that reduce the performance of neural networks (Biggio et al., 2013; Szegedy et al., 2014), has established itself as an important research area.

**Adversarial training** methods, such as PGD (Madry et al., 2018), compute concrete perturbations that maximize the training loss, before training the network on these samples. This can be seen as optimizing an under-approximation of the worst-case loss. While it empirically improves robustness significantly, it generally does not induce sufficient regularization for certification and has been shown to fail in the face of more powerful attacks (Tramèr et al., 2020).

**Neural Network Certification** rigorously proves a network’s adversarial robustness. While complete verification methods (Tjeng et al., 2019; Bunel et al., 2020; Zhang et al., 2022c; Ferrari et al., 2022) can decide every robustness

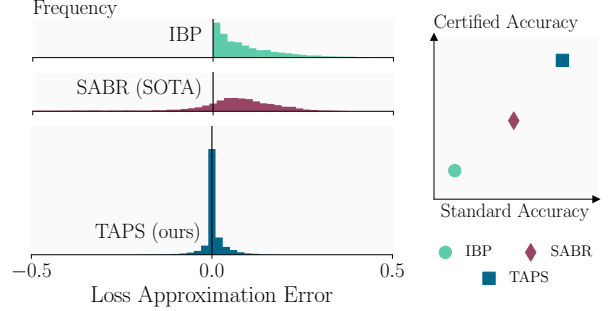


Figure 1: Histograms of the worst-case loss approximation errors over the test set (left) for different training methods show that TAPS (our work) achieves the most precise approximations and highest certified accuracy (right).

property given enough (exponential) time, incomplete methods (Wong & Kolter, 2018; Singh et al., 2019; Zhang et al., 2018) trade precision for scalability.

**Sound Certified Training** methods are empirically successful at increasing certified accuracies but induce over-regularization leading to severely reduced standard accuracies. These techniques generally optimize an upper bound on the worst-case loss, typically computed via a form of bound propagation (Mirman et al., 2018; Gowal et al., 2018; Wong & Kolter, 2018; Zhang et al., 2018; Shi et al., 2021). We illustrate this idea using the popular interval bound propagation (IBP) in Figure 1. There, we show histograms (left side) of the worst-case loss approximation error over the test set. Positive values (right of the y-axis) correspond to over-approximations and negative values (left of the y-axis) to under-approximations. On the right side, we illustrate the corresponding certified and standard accuracies. Sound methods (IBP: top left in Figure 1), by definition, always yield over-approximations (positive errors) of the optimization objective, *i.e.*, the true worst-case loss. Intuitively, this leads to already robust points inducing high losses, resulting in over-regularization and thus reduced network capacity for the remaining not yet robust points, which in turn reduces accuracy (right in Figure 1).

**Unsound Certified Training** methods reduce this over-regularization by sacrificing the soundness of the worst-case loss over-approximations in favor of more precise but not necessarily sound approximations. This tends to result in

<sup>1</sup>Department of Computer Science, ETH Zurich. Correspondence to: Yuhao Mao <yuhmao@ethz.ch>.

networks that achieve higher standard and certified accuracies, but can be harder to verify (Balunovic & Vechev, 2020; Palma et al., 2022; Müller et al., 2022a). Recent advances in certification techniques, however, have made their certification possible (Ferrari et al., 2022; Zhang et al., 2022c). We illustrate this idea for SABR in Figure 1, where we observe a 6-fold reduction in the mean worst-case loss approximation error (middle left), leading to reduced regularization and yielding a more accurate network (right).

**This Work** proposes TAPS<sup>1</sup>, a novel (unsound) certified training method which yields precise worst-case loss approximations, reducing over-regularization and thus increasing certified and standard accuracies. Compared to SABR (the current state-of-the-art) in Figure 1, TAPS enjoys a further 5-fold mean approximation error reduction and significantly reduced variance (bottom left), leading to improved certified and natural accuracies (right). The key technical insight behind TAPS is to combine IBP and PGD training via a gradient connector, a novel mechanism which allows for joint training, such that over-approximation errors of IBP and under-approximations of PGD cancel out. As we demonstrate empirically, TAPS yields exceptionally tight worst-case loss approximations and obtains state-of-the-art results on MNIST, CIFAR-10, and TINYIMAGENET.

## 2. Adversarial and Certified Training

Here we provide the necessary background on adversarial and certified training. We consider a classifier  $F: \mathcal{X} \mapsto \mathcal{Y}$  parameterized by weights  $\theta$  and predicting a class  $y_{\text{pred}} = F(\mathbf{x}) = \arg \max_{y \in \mathcal{Y}} f_y(\mathbf{x})$  for every input  $\mathbf{x} \in \mathcal{X} \subseteq \mathbb{R}^d$  with label  $y \in \mathcal{Y} = \{1, \dots, K\}$  where  $\mathbf{f}: \mathcal{X} \mapsto \mathbb{R}^{|\mathcal{Y}|}$  is a neural network, assigning a logit  $o_i := f_i(\mathbf{x})$  to each class  $i$ .

**Adversarial Robustness** We call a classifier adversarially robust on an  $\ell_p$ -norm ball  $\mathcal{B}_p(\mathbf{x}, \epsilon)$  if it classifies all elements within the ball to the correct class, i.e.,  $F(\mathbf{x}') = y$  for all perturbed inputs  $\mathbf{x}' \in \mathcal{B}_p(\mathbf{x}, \epsilon)$ . In this work, we focus on  $\ell_\infty$ -robustness with  $\mathcal{B}_\infty(\mathbf{x}, \epsilon) := \{\mathbf{x}' \mid \|\mathbf{x}' - \mathbf{x}\|_\infty \leq \epsilon\}$  and thus drop the subscript  $\infty$ .

**Neural Network Verification** is used to formally verify the robustness of a neural network for a given sample and robustness specification, i.e., to *prove* that all inputs in the region  $\mathcal{B}(\mathbf{x}, \epsilon)$  yield the correct classification. We call such samples  $\mathbf{x}$  certifiably robust and denote the portion of such samples as *certified accuracy*, forming a lower bound to the true robustness.

Interval bound propagation (IBP) (Mirman et al., 2018; Gowal et al., 2018) is a particularly simple yet effective verification method. Conceptually, it computes over-

approximations of a network’s reachable set by propagating the input region  $\mathcal{B}(\mathbf{x}, \epsilon)$  through the network. Then, it checks whether all outputs in the thus obtained reachable set yield the correct classification. This propagation sequentially computes a BOX over-approximation (each dimension is described as an interval) of a layer’s output, given a BOX input. As an example, consider an  $L$ -layer network  $\mathbf{f} = \mathbf{h}_L \circ \text{ReLU} \circ \mathbf{h}_{L-2} \circ \dots \circ \mathbf{h}_1$ , with linear layers  $\mathbf{h}$  and ReLU activation functions. Given an input region  $\mathcal{B}(\mathbf{x}, \epsilon)$ , we over-approximate it as a hyper-box  $[\underline{\mathbf{x}}^0, \overline{\mathbf{x}}^0]$ , centered at  $\mathbf{c}^0 := \mathbf{x}$  and with radius  $\delta^0 := \epsilon$ , such that we have the  $i^{\text{th}}$  dimension of the input  $x_i^0 \in [c_i^0 - \delta_i^0, c_i^0 + \delta_i^0]$ . Given a linear layer  $\mathbf{h}_i(\mathbf{x}^{l-1}) = \mathbf{W}\mathbf{x}^{l-1} + \mathbf{b} =: \mathbf{x}^l$ , we then obtain the hyper-box relaxation of its output defined by center  $\mathbf{c}^l = \mathbf{W}\mathbf{c}^{l-1} + \mathbf{b}$  and radius  $\delta^l = |\mathbf{W}|\delta^{l-1}$ , where  $|\cdot|$  denotes the elementwise absolute value. A ReLU activation  $\text{ReLU}(\mathbf{x}^{l-1}) := \max(0, \mathbf{x}^{l-1})$  can be relaxed by propagating the lower and upper bound separately, resulting in the output hyper-box  $[\text{ReLU}(\underline{\mathbf{x}}^{l-1}), \text{ReLU}(\overline{\mathbf{x}}^{l-1})]$ . Proceeding this way for all layers, we obtain lower and upper bounds on the network outputs  $[\underline{\mathbf{o}}, \overline{\mathbf{o}}]$  and can check if the score of the target class is greater than that of all other classes by computing upper bounds  $\overline{\mathbf{o}}^\Delta$  on the logit differences  $\mathbf{o}^\Delta := \mathbf{o} - o_y \mathbf{1}$ . Note that this is equivalent to showing that the maximum margin loss  $\mathcal{L}_{\text{MA}}(\mathbf{x}', y)$  is less than 0, or all perturbed inputs  $\mathbf{x}' \in \mathcal{B}(\mathbf{x}, \epsilon)$  where

$$\mathcal{L}_{\text{MA}}(\mathbf{x}, y) := \max_{i \neq y} \overline{o}_i^\Delta. \quad (1)$$

We note that other, more precise methods for bound computation exist (Singh et al., 2019; 2018; Xu et al., 2020; Zhang et al., 2020; Tjeng et al., 2019).

**Adversarial Training** is used to train neural networks  $\mathbf{f}$  with weights  $\theta$  that are *empirically* robust to adversarial examples, by solving the following optimization problem:

$$\theta = \arg \min_{\theta} \mathbb{E}_{\mathbf{x}, y} \left[ \max_{\hat{\mathbf{x}} \in \mathcal{B}(\mathbf{x}, \epsilon)} \mathcal{L}_{\text{CE}}(\hat{\mathbf{x}}, y) \right], \text{ where} \quad (2)$$

$$\mathcal{L}_{\text{CE}}(\mathbf{x}, y) := \ln \left( 1 + \sum_{i \neq y} \exp(f_i(\mathbf{x}) - f_y(\mathbf{x})) \right). \quad (3)$$

As the inner maximization objective in Equation (2) can generally not be solved exactly, adversarial training optimizes a lower bound by first computing concrete examples  $\hat{\mathbf{x}} \in \mathcal{B}(\mathbf{x}, \epsilon)$  that maximize this inner loss term and then training the network  $\theta$  with these samples. A well-established method for this is, so-called *Projected Gradient Descent* (PGD) training (Madry et al., 2018). Starting from a random initialization point  $\hat{\mathbf{x}}_0 \in \mathcal{B}(\mathbf{x}, \epsilon)$ , it performs  $N$  update steps  $\hat{\mathbf{x}}_{n+1} = \Pi_{\mathcal{B}(\mathbf{x}, \epsilon)} \hat{\mathbf{x}}_n + \eta \text{sign}(\nabla_{\hat{\mathbf{x}}_n} \mathcal{L}_{\text{CE}}(\hat{\mathbf{x}}_n, y))$  with step size  $\eta$  and projection operator  $\Pi$ . Networks trained this way typically exhibit good empirical robustness but remain hard to formally verify and vulnerable to stronger or different attacks (Tramèr et al., 2020; Croce & Hein, 2020).

<sup>1</sup>Training via Adversarial Propagation through Subnetworks

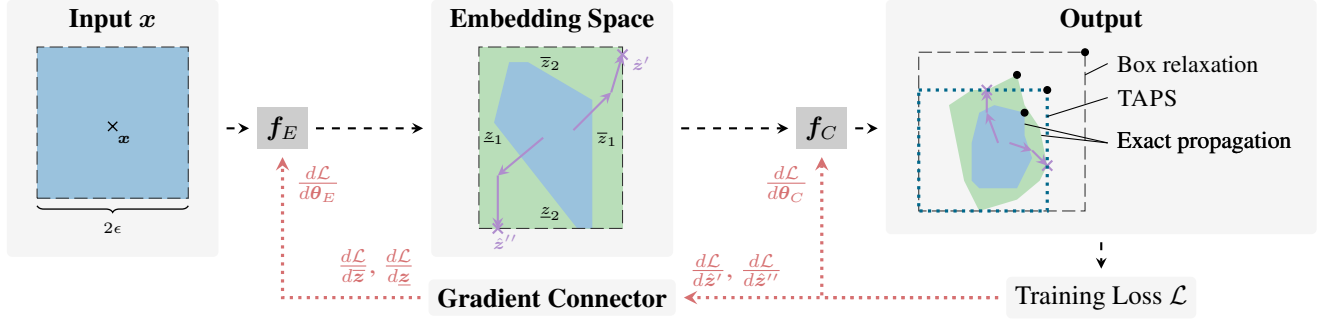


Figure 2: Overview of TAPS training. First, forward propagation ( $\rightarrow$ ) of a region  $B(x, \epsilon)$  (■, left) around an input  $x$  (×) through the feature extractor  $f_E$  yields the exact reachable set (■, middle) and its IBP approximation  $[z, \bar{z}]$  (□, middle) in the embedding space. Further IBP propagation through the classifier  $f_C$  would yield an imprecise box approximation (□, right) of the reachable set (■, right). Instead, TAPS conducts an adversarial attack ( $\rightarrow$ ) in the embedding space IBP approximation (■) yielding an under-approximation (□) of its reachable set (■, right). We illustrate the points realizing the worst-case loss in every output region with • and enable back-propagation ( $\rightarrow$ ) through the adversarial attack by introducing the gradient connector (discussed in Section 3.2).

**Certified Training** is used to train neural networks  $f$  with weights  $\theta$  that are *certifiably* robust to adversarial examples. To this end, methods in the *certification aligned* paradigm optimize an upper bound of the inner maximization objective in Equation (2), while *training aligned* methods aim to find a precise approximation. Often, methods in both paradigms are based on evaluating the  $\mathcal{L}_{CE}$  loss function with upper bounds  $\bar{\sigma}^\Delta$  on the logit differences, obtained via bound propagation as described above. Following the certification aligned paradigm, IBP, for example, uses sound BOX bounds on the logit differences, yielding the loss

$$\mathcal{L}_{IBP}(x, y, \epsilon) := \ln \left( 1 + \sum_{i \neq y} \exp(\bar{\sigma}_i^\Delta) \right). \quad (4)$$

SABR (Müller et al., 2022a), in contrast, belongs to the training aligned paradigm and achieves a more precise (although not sound) worst-case loss approximation  $\mathcal{L}_{IBP}(x', y, \tau)$  by not propagating the whole input region  $B(x, \epsilon)$  but only an adversarially selected subset  $B(x', \tau) \subset B(x, \epsilon)$  with  $\tau < \epsilon$ . This reduces approximation errors (see Figure 5) and thus regularization, leading to improved certified and standard accuracy.

Orthogonally, COLT (Balunovic & Vechev, 2020) uses the tighter ZONOTOPE (Singh et al., 2019) instead of BOX bounds combined with adversarial training to reduce approximation errors: Balunovic & Vechev (2020) split a network into two parts  $f = f_2 \circ f_1$ . During every stage of training, they now fix the weights  $\theta_1$  of  $f_1$  and only train  $f_2$  as follows: First, they compute a ZONOTOPE over-approximation of the reachable set of  $f_1$ . Then, they conduct adversarial training of the remaining network  $f_2$  within the thus obtained bounds. They repeat this process in stages, at first assigning the whole network to  $f_2$ , before slowly moving this interface between ZONOTOPE and PGD propagation through the network. Crucially, they do not facilitate the

computation of any gradients with respect to  $f_1$ . Thus the weights of  $\theta_1$  are effectively frozen and  $f_2$  is trained to be robust to approximation errors of  $f_1$ . However,  $f_1$  is *not* trained to minimize these approximation errors. This makes training very slow and limited to small networks (even for certified training methods).

### 3. Precise Worst-Case Loss Approximation

In this section, we introduce TAPS, our novel certified training method combining IBP and PGD training to obtain precise worst-case loss estimates while permitting joint training and inducing a well-behaved optimization problem.

#### 3.1. TAPS

The key insight behind TAPS is that adversarial training with PGD and certified training with IBP complement each other perfectly: First, both yield well-behaved optimization problems, as witnessed by their empirical success and second, we can combine them such that the over-approximation errors incurred during IBP are compensated by the under-approximations of PGD. We do this as follows: For every sample, we first propagate the input region part-way through the network using IBP and then conduct PGD training within the thus obtained BOX approximation. The key technical challenge with this approach (and the main difference to COLT (Balunovic & Vechev, 2020)) is that we connect the gradients of the two approaches, enabling joint training. We illustrate this in Figure 2.

In more detail, we partition a neural network  $f$  with weights  $\theta$  into a *feature extractor*  $f_E$  and *classifier*  $f_C$  with parameters  $\theta_E$  and  $\theta_C$ , respectively, such that we have  $f_\theta = f_C \circ f_E$  and  $\theta = \theta_E \cup \theta_C$ . We refer to the output space of the feature extractor as the *embedding space*.

Given an input sample  $x$  (illustrated as  $\times$  in Figure 2) and a corresponding input region  $\mathcal{B}(x, \epsilon)$  (■ in the input panel), training proceeds as follows: During the forward pass ( $\rightarrow$ ), we first use IBP to compute a box over-approximation  $[\underline{z}, \bar{z}]$  (□) of the feature extractor’s exact reachable set (■), shown in the middle panel of Figure 2. Then, we conduct separate adversarial attacks ( $\rightarrow$ ) in this embedding space (■) to bound all output dimensions of the classifier, yielding latent adversarial examples  $\hat{z} \in [\underline{z}, \bar{z}]$ . This way, we *under-approximate* the classifier, partially compensating the IBP over-approximation of the feature extractor and yielding the dotted box □ in the output space. Full IBP propagation, in contrast, continues to exponentially accumulate approximation errors (Müller et al., 2022a; Shi et al., 2021), yielding the much larger dashed box □. We now compute the TAPS loss  $\mathcal{L}_{\text{TAPS}}$  analogously to  $\mathcal{L}_{\text{IBP}}$  (Equation (4)) by plugging the TAPS bound estimate (□) into the Cross-Entropy loss. Comparing the resulting losses (illustrated as • and growing towards the top right), we see that while the TAPS bounds are not necessarily sound, they yield a much better approximation of the true worst-case loss.

During the backward pass ( $\leftarrow$  in Figure 2), we compute the gradients w.r.t. the classifier’s parameters  $\theta_C$  and the latent adversarial examples  $\hat{z}$  (classifier input) as usual. However, to compute the gradients w.r.t. the feature extractor’s parameters  $\theta_F$ , we have to compute (pseudo) gradients of the latent adversarial examples  $\hat{z}$  w.r.t. the box bounds  $\underline{z}$  and  $\bar{z}$ . As these gradients are not well defined, we introduce the *gradient connector*, discussed next, as an interface between the feature extractor’s output and the classifier’s input to impose pseudo gradients. This allows us to train  $f_E$  and  $f_C$  jointly, leading to a feature extractor that minimizes approximation errors and a classifier that is resilient to the spurious points included in the remaining approximation errors.

### 3.2. Gradient Connector

The key function of the gradient connector is to enable gradient computation through the adversarial example search in the embedding space. Using the chain rule, this only requires us to define the (pseudo) gradients  $\frac{\partial \hat{z}}{\partial \underline{z}}$  and  $\frac{\partial \hat{z}}{\partial \bar{z}}$  of the latent adversarial examples  $\hat{z}$  w.r.t. the box bounds  $[\underline{z}, \bar{z}]$  on the feature extractor’s outputs. Below, we will focus on the  $i^{\text{th}}$  dimension of the lower box bound and note that all other dimensions and the upper bounds follow analogously.

As the latent adversarial examples can be seen as multivariate functions in the box bounds, we obtain the general form  $\frac{d\mathcal{L}}{dz_i} = \sum_j \frac{d\mathcal{L}}{d\hat{z}_j} \frac{\partial \hat{z}_j}{\partial z_i}$ , depending on all dimensions of the latent adversarial example. However, as a box approximation does not encode any information on the dependence between dimensions, we, intuitively, want the gradients w.r.t. the  $i^{\text{th}}$  dimension of the box bounds  $\underline{z}_i$  to only depend on the corresponding dimension of the latent adversarial ex-

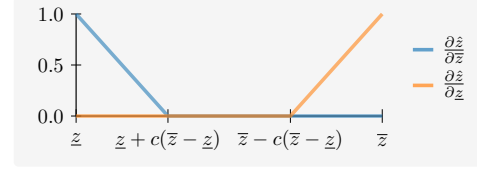


Figure 3: Gradient connector visualization for  $c = 0.3$ .

ample  $\hat{z}_i$ . Therefore, we set  $\frac{\partial \hat{z}_j}{\partial z_i} = 0$  for  $i \neq j$  and obtain  $\frac{d\mathcal{L}}{dz_i} = \frac{d\mathcal{L}}{d\hat{z}_i} \frac{\partial \hat{z}_i}{\partial z_i}$ , leaving only  $\frac{\partial \hat{z}_i}{\partial z_i}$  for us to define.

The most natural and mathematically correct gradient connector is the *binary connector*, i.e., set  $\frac{\partial \hat{z}_i}{\partial z_i} = 1$  when  $\hat{z}_i = \underline{z}_i$  and 0 otherwise. However, the latent adversarial input often does not lie on a corner (extremal vertex) of the bounding box, leading to sparse gradients and thus a less well-behaved optimization problem. More importantly, the binary connector is very sensitive to the distance between (local) loss extrema and the box boundary and thus inherently ill-suited to gradient-based optimization. For example, a local extremum at  $\hat{z}_i$  would induce  $\frac{\partial \hat{z}_i}{\partial z_i} = 1$  in the box  $[\hat{z}_i, 0]$ , but  $\frac{\partial \hat{z}_i}{\partial z_i} = 0$  for  $[\hat{z}_i - \epsilon, 0]$ , even for arbitrarily small  $\epsilon$ .

To alleviate both of these problems, we consider a *linear connector*, i.e., set  $\frac{\partial \hat{z}_i}{\partial z_i} = \frac{\bar{z}_i - \hat{z}_i}{\bar{z}_i - \underline{z}_i}$ . However, even when our latent adversarial example is very close to one bound, the linear connector would induce non-zero gradients w.r.t. to the opposite bound. To remedy this undesirable behavior, we propose the *rectified linear connector*, setting  $\frac{\partial \hat{z}_i}{\partial z_i} = \max(0, 1 - \frac{\hat{z}_i - \underline{z}_i}{c(\bar{z}_i - \underline{z}_i)})$  where  $c \in [0, 1]$  is a constant. We visualize it for  $c = 0.3$  in Figure 3 and note that it recovers the binary connector for  $c = 0$  and the linear connector for  $c = 1$ . To prevent gradient sparsity ( $c \leq 0.5$ ) while avoiding the above-mentioned counterintuitive gradient connections ( $c \geq 0.5$ ), we set  $c = 0.5$  unless indicated otherwise. This ensures that, for every dimension, exactly one of the bounds has a non-zero gradient, unless our latent adversarial input is centered between them, i.e.,  $\hat{z}_i = (\underline{z}_i + \bar{z}_i)/2$ , where both have zero gradients.

To avoid numerical instability when the upper and lower bounds are identical in the  $i^{\text{th}}$  dimension, i.e.,  $\underline{z}_i = \bar{z}_i$ , we set  $\frac{\partial \hat{z}_i}{\partial z_i} = \max(0, 1 - \frac{\max(\hat{z}_i - \underline{z}_i, \delta/2)}{\max(c(\bar{z}_i - \underline{z}_i), \delta)})$ , where  $\delta = 10^{-5}$  is a small positive constant. Observe that this clipping is negligible unless the lower and the upper bounds are very close while yielding  $\frac{\partial \hat{z}_i}{\partial z_i} = \frac{\partial \hat{z}_i}{\partial \bar{z}_i} = 0.5$  when they are identical, thus turning the gradient connector into an identity function.

As outlined before, our approach is conceptually similar to COLT (Balunovic & Vechev, 2020). However, our construction and gradient connector allow us to overcome the main issue of COLT, i.e., that gradients do not flow into the earlier part of the neural network – in our case  $f_E$ .

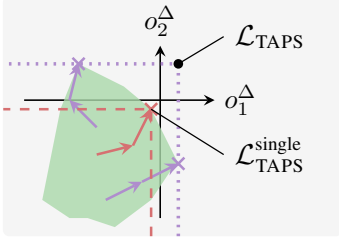


Figure 4: Illustration of the bounds on  $o_i^\Delta := o_i - o_t$  obtained via single estimator (---) and multi-estimator (···) PGD and the points maximizing the corresponding losses:  $\times$  for  $\mathcal{L}_{\text{TAPS}}^{\text{single}}$  and  $\bullet$  for  $\mathcal{L}_{\text{TAPS}}$ .

### 3.3. TAPS Loss & Multi-estimator PGD

The standard PGD attack, used in adversarial training, henceforth called *single-estimator* PGD, is based on maximizing the Cross-Entropy loss  $\mathcal{L}_{\text{CE}}$  (Equation (3)) of a single input. In the context of TAPS, this results in the overall loss

$$\mathcal{L}_{\text{TAPS}}^{\text{single}}(x, y, \epsilon) = \max_{\hat{z} \in [\underline{z}, \bar{z}]} \ln \left( 1 + \sum_{i \neq y} \exp(f_C(\hat{z})_i - f_C(\hat{z})_y) \right),$$

where the embedding space bounding box  $[\underline{z}, \bar{z}]$  is obtained via IBP. However, this loss is not well aligned with the robustness objective (Equation (1)). Consider the example illustrated in Figure 4, where only points in the lower-left quadrant are classified correctly (as  $o_i^\Delta := o_i - o_y < 0$ ). We compute the latent adversarial example  $\hat{z}$  by conducting a standard adversarial attack on the Cross-Entropy loss (optimally for illustration purposes) over the reachable set  $\blacksquare$  and observe that the corresponding output  $f(\hat{z})$  ( $\times$ ) is classified correctly. However, if we instead use the logit differences  $o_1^\Delta$  and  $o_2^\Delta$  as attack objectives, we obtain two misclassified points ( $\times$ ). We combine their dimension-wise worst-case bounds (···) to obtain the point  $\bullet$ , which is equivalent to the maximum loss point in an optimal box approximation. As this directly corresponds to true robustness, we propose the *multi-estimator* PGD variant of  $\mathcal{L}_{\text{TAPS}}$ , which estimates the upper bounds on the logit differences  $o_i^\Delta$  using separate samples and then computes the loss function using the per-dimension worst-cases as:

$$\mathcal{L}_{\text{TAPS}}(x, y, \epsilon) = \ln \left( 1 + \sum_{i \neq y} \exp \left( \max_{\hat{z} \in [\underline{z}, \bar{z}]} f_C(\hat{z})_i - f_C(\hat{z})_y \right) \right).$$

### 3.4. Training Objective & Regularization

While complete certification methods can decide any robustness property, they can require exponential time. Therefore, networks should not only be regularized to be robust but certifiable as well. Thus, we propose to combine the IBP loss for easy-to-learn and certify samples with the TAPS loss for harder samples as follows:

$$\mathcal{L}(x, y, \epsilon) = \mathcal{L}_{\text{TAPS}}(x, y, \epsilon) \cdot \mathcal{L}_{\text{IBP}}(x, y, \epsilon).$$

This expresses that every sample should be either certifiable with TAPS or IBP bounds<sup>2</sup>. Further, as by construction  $\mathcal{L}_{\text{TAPS}} \leq \mathcal{L}_{\text{IBP}}$ , we add a scaling term to the loss gradient  $\alpha$ :

$$\frac{d\mathcal{L}}{d\theta} := \alpha \frac{d\mathcal{L}_{\text{TAPS}}}{d\theta} \cdot \mathcal{L}_{\text{IBP}} + (1 - \alpha) \frac{d\mathcal{L}_{\text{IBP}}}{d\theta} \cdot \mathcal{L}_{\text{TAPS}}.$$

Here  $\alpha = 0$  and  $\alpha = 1$  correspond to (weighted) IBP and TAPS gradients only, respectively. Henceforth, we express this as the regularization weight  $w_{\text{TAPS}} = \frac{\alpha}{1-\alpha}$ , which intuitively expresses the weight put on TAPS, and use  $w_{\text{TAPS}} = 5$  unless specified otherwise. Lastly, we reduce the variance of  $\mathcal{L}$  by averaging  $\mathcal{L}_{\text{IBP}}$  and  $\mathcal{L}_{\text{TAPS}}$  over a data batch before multiplying (see App. A).

## 4. Experimental Evaluation

In this section, we evaluate TAPS empirically. First, we compare it to a range of state-of-the-art certified training methods before conducting an extensive ablation study.

### 4.1. Experimental setup

We implement TAPS in PyTorch (Paszke et al., 2019) and use MN-BAB (Ferrari et al., 2022) for certification. We conduct experiments on MNIST (LeCun et al., 2010), CIFAR-10 (Krizhevsky et al., 2009), and TINYIMAGENET (Le & Yang, 2015) using the challenging  $\ell_\infty$  perturbations and a 7-layer convolutional architecture CNN7 (Shi et al., 2021; Müller et al., 2022a). For more details, see App. B.

### 4.2. Main Results

In Table 1, we compare TAPS to state-of-the-art certified training methods. The most closely related ones are IBP, recovered by TAPS if the classifier size is zero, and COLT, which also combines bound propagation with adversarial attacks but does not allow for joint training. TAPS dominates IBP, improving on its certified and natural accuracy in all settings and demonstrating the importance of avoiding over-regularization. Compared to COLT, TAPS improves certified accuracies significantly, highlighting the importance of joint optimization. In some settings, this comes at the cost of slightly reduced natural accuracy, potentially due to COLT’s use of the more precise ZONOTOPE approximations. Compared to the recent SABR and IBP-R, we observe that TAPS often achieves higher certified accuracies at the cost of slightly reduced natural accuracies. We, therefore, combine TAPS with SABR, by replacing the IBP portion of TAPS with SABR propagation to yield STAPS. STAPS then achieves better certified accuracies in almost all settings and better natural accuracies in many.

<sup>2</sup>See Fischer et al. (2019) for further discussion.



Table 1: Comparison of natural (Nat.) and certified (Cert.) accuracy over certified training methods on the MNIST, CIFAR-10, and TINYIMAGENET test sets. We report results for other methods from the relevant literature.

Dataset	$\epsilon_\infty$	Training Method	Source	Nat. [%]	Cert. [%]
MNIST	0.1	COLT	Balunovic & Vechev (2020)	99.2	97.1
		CROWN-IBP	Zhang et al. (2020)	98.83	97.76
		IBP	Shi et al. (2021)	98.84	97.95
		SABR	Müller et al. (2022a)	<b>99.25</b>	98.06
		TAPS	this work	99.19	<b>98.39</b>
		STAPS	this work	99.15	98.37
	0.3	COLT	Balunovic & Vechev (2020)	97.3	85.7
		CROWN-IBP	Zhang et al. (2020)	98.18	92.98
		IBP	Shi et al. (2021)	97.67	93.10
		SABR	Müller et al. (2022a)	<b>98.82</b>	93.38
		TAPS	this work	97.94	<b>93.62</b>
		STAPS	this work	98.53	93.51
CIFAR-10	$\frac{2}{255}$	COLT	Balunovic & Vechev (2020)	78.4	60.5
		CROWN-IBP	Zhang et al. (2020)	71.52	53.97
		IBP	Shi et al. (2021)	66.84	52.85
		IBP-R	Palma et al. (2022)	78.19	61.97
		SABR	Müller et al. (2022a)	79.52	62.57
		TAPS	this work	75.09	61.56
		STAPS	this work	<b>79.76</b>	<b>62.98</b>
	$\frac{8}{255}$	COLT	Balunovic & Vechev (2020)	51.7	27.5
		CROWN-IBP	Xu et al. (2020)	46.29	33.38
		IBP	Shi et al. (2021)	48.94	34.97
		IBP-R	Palma et al. (2022)	51.43	27.87
		SABR	Müller et al. (2022a)	52.00	<b>35.25</b>
		TAPS	this work	49.76	35.10
		STAPS	this work	<b>52.82</b>	34.65
TINYIMAGENET	$\frac{1}{255}$	CROWN-IBP	Shi et al. (2021)	25.62	17.93
		IBP	Shi et al. (2021)	25.92	17.87
		SABR	Müller et al. (2022a)	28.64	20.34
		TAPS	this work	28.34	20.82
		STAPS	this work	<b>28.98</b>	<b>22.16</b>

In Table 2, we compare TAPS to SORTNET, a generalization of a range of recent architectures (Zhang et al., 2021; 2022a; Anil et al., 2019), introducing novel activation functions tailored to yield networks with high  $\ell_\infty$ -robustness. While SORTNET performs well on CIFAR-10 at  $\epsilon = 8/255$ , it is dominated by STAPS in every other setting, especially at smaller perturbation magnitudes.

### 4.3. Ablation Study

**Approximation Precision** To evaluate whether TAPS yields more precise approximations of the worst-case loss than other certified training methods, we train a small CNN3 on MNIST using IBP, SABR, and TAPS and compute approximations of the maximum margin loss with IBP, PGD (50 steps 3 restarts), SABR (tuned to  $\lambda = 0.4$ ), and TAPS for all test set samples. We report histograms over the difference to the exact worst-case loss computed with a MILP en-

Table 2: Comparison of natural (Nat.) and certified (Cert.) accuracy [%] to SORTNET (Zhang et al., 2022b).

Dataset	$\epsilon$	SORTNET		STAPS (ours)	
		Nat.	Cert.	Nat.	Cert.
MNIST	0.1	99.01	98.14	<b>99.15</b>	<b>98.37</b>
	0.3	98.46	93.40	<b>98.53</b>	<b>93.51</b>
CIFAR-10	2/255	67.72	56.94	<b>79.76</b>	<b>62.98</b>
	8/255	<b>54.84</b>	<b>40.39</b>	52.82	34.65
TINYIMAGENET	1/255	25.69	18.18	<b>28.98</b>	<b>22.16</b>

coding (Tjeng et al., 2019) in Figure 5 and note that positive values corresponding to over-approximations while negative values correspond to under-approximation. We observe that regardless of the training method, the TAPS approximation is by far the most precise, achieving the smallest mean and mean absolute error as well as variance.

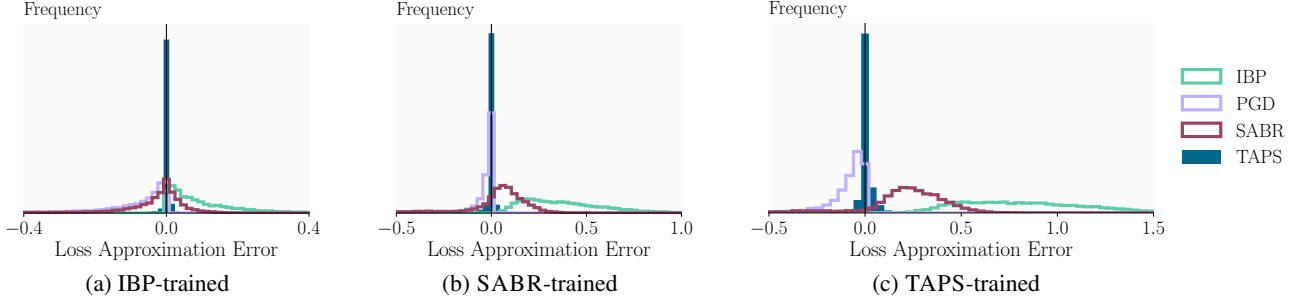


Figure 5: Distribution of the worst-case loss approximation errors over test set samples, depending on the training and bounding method. Positive values correspond to over-approximations and negative values to under-approximations. We use an exact MILP encoding (Tjeng et al., 2019) as reference.

Table 3: Effect of IBP regularization and the TAPS gradient expanding coefficient  $\alpha$  for MNIST  $\epsilon = 0.3$ .

$w_{\text{TAPS}}$	Avg time (s)	Nat (%)	Adv. (%)	Cert. (%)
$\mathcal{L}_{\text{IBP}}$	2.3	97.6	93.37	93.15
0	2.7	97.37	93.32	93.06
1	4.5	97.86	93.80	93.36
5	6.9	98.16	94.18	<b>93.55</b>
10	15.7	98.25	94.43	93.02
15 <sup>†</sup>	42.8	98.53	<b>95.00</b>	91.55
20 <sup>†</sup>	73.7	<b>98.75</b>	94.33	82.67
$\infty^{\dagger}$	569.7	98.0	94.00	45.00
$\mathcal{L}_{\text{TAPS}}^{\dagger}$	817.1	98.5	94.50	17.50

<sup>†</sup> Only evaluated on part of the test set within a 2-day time limit.

**IBP Regularization** To analyze the effectiveness of the multiplicative IBP regularization discussed in Section 3.4, we train with IBP in isolation ( $\mathcal{L}_{\text{IBP}}$ ), IBP with TAPS loss weighted gradients ( $w_{\text{TAPS}} = 0$ ), varying levels of gradient scaling for the TAPS component ( $w_{\text{TAPS}} \in [1, 20]$ ), TAPS with IBP loss weighting ( $w_{\text{TAPS}} = \infty$ ), and TAPS in isolation.

We observe that IBP in isolation yields comparatively low standard and adversarial but moderate certified accuracies with fast certification times. Increasing the weight  $w_{\text{TAPS}}$  of the TAPS gradients reduces regularization, leading to longer certification times. Initially, this also translates to higher adversarial and certified accuracies, peaking at  $w_{\text{TAPS}} = 15$  and  $w_{\text{TAPS}} = 5$ , respectively, before especially certified accuracy decreases as regularization becomes insufficient for certification.

**Split Location** TAPS splits a given network into a feature extractor and classifier, which are then approximated using IBP and PGD, respectively. As IBP propagation accumulates over-approximation errors while PGD is an under-approximation, the location of this split has a strong impact on the regularization level induced by TAPS. To analyze this effect, we train multiple CNNs such that we obtain classifiers with between 0 and 6 (all) ReLUs and

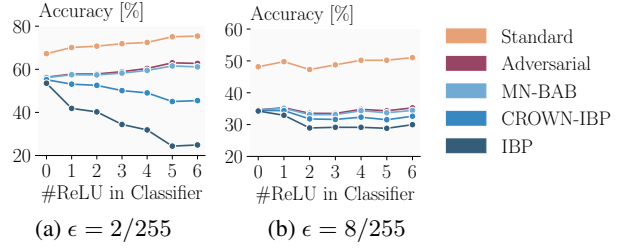


Figure 6: Effect of split location on the standard and robust accuracy of TAPS trained networks, depending on the perturbation magnitude  $\epsilon$  for different certification methods for CIFAR-10. 0 ReLUs in the classifier recovers IBP training.

illustrate the resulting standard, adversarial, and certified (using different methods) accuracies in Figure 6.

For small perturbations ( $\epsilon = 2/255$ ), natural and adversarial accuracy increase with classifier size and thus decreasing regularization. While the precise MN-BAB certification can translate this into increasing certified accuracies up to large classifier sizes, regularization quickly becomes insufficient for the less precise IBP and CROWN-IBP certification, leading to dropping certified accuracies. For larger perturbations ( $\epsilon = 8/255$ ), the behavior is more complex with an initial increase of all accuracies with classifier size being followed by a sudden drop and a slow recovery. We hypothesize that this effect is due to the IBP regularization starting to dominate optimization. We observe increased training difficulty as well (see App. C for details). For both perturbation magnitudes, gains in certified accuracy can only be realized with the precise MN-BAB certification (Müller et al., 2022a), highlighting the importance of recent developments in neural network verification for certified training.

**Gradient Connector** In Figure 7, we illustrate the effect of our gradient connector’s parameterization (Section 3.2) on training. We report TAPS accuracy (portion of samples where all latent adversarial examples are classified correctly)

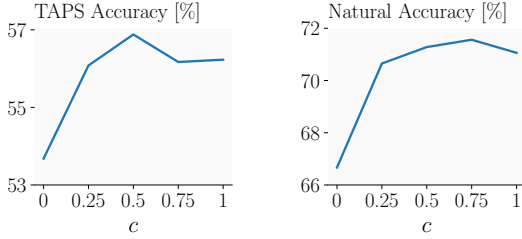


Figure 7: Effect of the gradient connector parameter  $c$  on TAPS (left) and natural (right) accuracy.

as a proxy for the goodness of fit. Recall that  $c = 0$  corresponds to the binary connector and  $c = 1$  to the linear connector. We observe that the binary connector achieves poor TAPS and natural accuracy, indicating a less well-behaved optimization problem. TAPS accuracy peaks at  $c = 0.5$ , indicating high goodness-of-fit and thus a well-behaved optimization problem. This agrees well with our theoretical considerations aiming to avoid sparsity ( $c < 0.5$ ) and contradicting gradients ( $c > 0.5$ ).

**Single-Estimator vs Multi-Estimator PGD** To evaluate the importance of our proposed multi-estimator PGD, we compare its performance to single-estimator PGD across a range of split positions, reporting results in Table 4. We observe that across all split positions, multi-estimator PGD achieves better certified and better or equal natural accuracy. Further, training collapses reproducibly for single-estimator PGD for small classifiers, indicating that multi-estimator PGD additionally improves training stability.

## 5. Related Work

**Verification Methods** In this work, we only consider deterministic verification methods, which analyze a given network as is. While *complete* (or *exact*) methods (Tjeng et al., 2019; Palma et al., 2021; Wang et al., 2021; Müller et al., 2022b; Zhang et al., 2022c) can decide any robustness property given enough time, *incomplete* methods (Singh et al., 2018; Raghunathan et al., 2018; Dathathri et al., 2020) sacrifice some precision for better scalability. However, recent complete methods can be used with a timeout to obtain effective incomplete methods.

**Certified Training** Most certified training methods compute and minimize sound over-approximations of the worst-case loss using different approximation methods: DIFFAI (Mirman et al., 2018) and IBP (Gowal et al., 2018) use BOX approximations, Wong et al. (2018) use DEEPZ relaxations (Singh et al., 2018), Wong & Kolter (2018) back-substitute linear bounds using fixed relaxations, Zhang et al. (2020) use dynamic relaxations (Zhang et al., 2018; Singh et al., 2019) and compute intermediate bounds using BOX relax-

Table 4: Comparison of TAPS training with single-estimator and multi-estimator PGD propagation, depending on the number of ReLUs in the network’s classifier portion.

# ReLU in Classifier	Single		Multiple	
	Certified	Natural	Certified	Natural
1	-†	31.47†	<b>93.62</b>	97.94
3	92.91	98.56	93.03	98.63
6	92.41	<b>98.88</b>	92.70	<b>98.88</b>

† Training encounters mode collapse. Last epoch performance reported.

ations. Shi et al. (2021) significantly shorten training schedules by combining IBP training with a special initialization. Some more recent methods instead compute and optimize more precise, but not necessarily sound, worst-case loss approximations: SABR (Müller et al., 2022a) reduce the regularization of IBP training by propagating only small but carefully selected subregions. IBP-R (Palma et al., 2022) combines adversarial training with large perturbation radii and an IBP-based regularization. COLT (Balunovic & Vechev, 2020) propagates DEEPZ relaxation through part of the network, before conducting adversarial attacks in the resulting latent space. However, in contrast to TAPS, COLT does not enable gradient flow between these components, preventing joint training. In our experimental evaluation (Section 4.2), we compare TAPS in detail to the above methods.

**Robustness by Construction** Li et al. (2019), Lécuyer et al. (2019), and Cohen et al. (2019) construct probabilistic classifiers by introducing randomness into the inference process of a base classifier. This allows them to derive robustness guarantees with high probability at the cost of significant (100x) runtime penalties. Zhang et al. (2021; 2022a) introduce  $\ell_\infty$ -distance neurons, generalized to SORT-NET by Zhang et al. (2022b) which inherently exhibits  $\ell_\infty$ -Lipschitzness properties, yielding good robustness for large perturbation radii, but poor performance for smaller ones.

## 6. Conclusion

We propose TAPS, a novel certified training method that reduces over-regularization by constructing and optimizing a precise worst-case loss approximation based on a combination of IBP and PGD training. Crucially, TAPS enables joint training over the IBP and PGD approximated components by introducing the gradient connector to define a gradient flow through their interface. Empirically, we confirm that TAPS yields much more precise approximations of the worst-case loss than existing methods, and demonstrate that this translates to state-of-the-art performance in certified training.



## References

- Anil, C., Lucas, J., and Grosse, R. B. Sorting out lipschitz function approximation. In *Proc. of International Conference on Machine Learning (ICML)*, volume 97, 2019.
- Balunovic, M. and Vechev, M. T. Adversarial training and provable defenses: Bridging the gap. In *Proc. of International Conference on Learning Representations (ICLR)*, 2020.
- Biggio, B., Corona, I., Maiorca, D., Nelson, B., Srndic, N., Laskov, P., Giacinto, G., and Roli, F. Evasion attacks against machine learning at test time. In *Machine Learning and Knowledge Discovery in Databases - European Conference, ECML PKDD 2013, Prague, Czech Republic, September 23-27, 2013, Proceedings, Part III*, volume 8190, 2013. doi: 10.1007/978-3-642-40994-3\_25.
- Bunel, R., Lu, J., Turkaslan, I., Torr, P. H. S., Kohli, P., and Kumar, M. P. Branch and bound for piecewise linear neural network verification. *J. Mach. Learn. Res.*, 21, 2020.
- Cohen, J. M., Rosenfeld, E., and Kolter, J. Z. Certified adversarial robustness via randomized smoothing. In *Proc. of International Conference on Machine Learning (ICML)*, volume 97, 2019.
- Croce, F. and Hein, M. Reliable evaluation of adversarial robustness with an ensemble of diverse parameter-free attacks. In *Proc. of International Conference on Machine Learning (ICML)*, volume 119, 2020.
- Dathathri, S., Dvijotham, K., Kurakin, A., Raghunathan, A., Uesato, J., Bunel, R., Shankar, S., Steinhardt, J., Goodfellow, I. J., Liang, P., and Kohli, P. Enabling certification of verification-agnostic networks via memory-efficient semidefinite programming. In *Neural Information Processing Systems (NeurIPS)*, 2020.
- Ferrari, C., Müller, M. N., Jovanovic, N., and Vechev, M. T. Complete verification via multi-neuron relaxation guided branch-and-bound. In *ICLR*, 2022.
- Fischer, M., Balunovic, M., Drachsler-Cohen, D., Gehr, T., Zhang, C., and Vechev, M. T. DL2: training and querying neural networks with logic. In *Proc. of International Conference on Machine Learning (ICML)*, volume 97, 2019.
- Gowal, S., Dvijotham, K., Stanforth, R., Bunel, R., Qin, C., Uesato, J., Arandjelovic, R., Mann, T. A., and Kohli, P. On the effectiveness of interval bound propagation for training verifiably robust models. *ArXiv preprint*, abs/1810.12715, 2018.
- Krizhevsky, A., Hinton, G., et al. Learning multiple layers of features from tiny images. 2009.
- Le, Y. and Yang, X. S. Tiny imagenet visual recognition challenge. *CS 231N*, 7(7), 2015.
- LeCun, Y., Cortes, C., and Burges, C. Mnist handwritten digit database. *ATT Labs [Online]*. Available: <http://yann.lecun.com/exdb/mnist>, 2, 2010.
- Lécuyer, M., Atlidakis, V., Geambasu, R., Hsu, D., and Jana, S. Certified robustness to adversarial examples with differential privacy. In *Symposium on Security and Privacy (SSP)*, 2019. doi: 10.1109/SP.2019.00044.
- Li, B., Chen, C., Wang, W., and Carin, L. Certified adversarial robustness with additive noise. In *Neural Information Processing Systems (NeurIPS)*, 2019.
- Madry, A., Makelov, A., Schmidt, L., Tsipras, D., and Vladu, A. Towards deep learning models resistant to adversarial attacks. In *Proc. of International Conference on Learning Representations (ICLR)*, 2018.
- Mirman, M., Gehr, T., and Vechev, M. T. Differentiable abstract interpretation for provably robust neural networks. In *Proc. of International Conference on Machine Learning (ICML)*, volume 80, 2018.
- Müller, M. N., Eckert, F., Fischer, M., and Vechev, M. T. Certified training: Small boxes are all you need. *CoRR*, abs/2210.04871, 2022a.
- Müller, M. N., Makarchuk, G., Singh, G., Püschel, M., and Vechev, M. T. PRIMA: general and precise neural network certification via scalable convex hull approximations. *Proc. ACM Program. Lang.*, 6(POPL), 2022b. doi: 10.1145/3498704.
- Palma, A. D., Behl, H. S., Bunel, R. R., Torr, P. H. S., and Kumar, M. P. Scaling the convex barrier with active sets. In *Proc. of International Conference on Learning Representations (ICLR)*, 2021.
- Palma, A. D., Bunel, R., Dvijotham, K., Kumar, M. P., and Stanforth, R. IBP regularization for verified adversarial robustness via branch-and-bound. *ArXiv preprint*, abs/2206.14772, 2022.
- Paszke, A., Gross, S., Massa, F., Lerer, A., Bradbury, J., Chanan, G., Killeen, T., Lin, Z., Gimelshein, N., Antiga, L., Desmaison, A., Köpf, A., Yang, E., DeVito, Z., Raison, M., Tejani, A., Chilamkurthy, S., Steiner, B., Fang, L., Bai, J., and Chintala, S. Pytorch: An imperative style, high-performance deep learning library. In *Neural Information Processing Systems (NeurIPS)*, 2019.

- Raghunathan, A., Steinhardt, J., and Liang, P. Certified defenses against adversarial examples. In *Proc. of International Conference on Learning Representations (ICLR)*, 2018.
- Shi, Z., Wang, Y., Zhang, H., Yi, J., and Hsieh, C. Fast certified robust training with short warmup. In *Neural Information Processing Systems (NeurIPS)*, 2021.
- Singh, G., Gehr, T., Mirman, M., Püschel, M., and Vechev, M. T. Fast and effective robustness certification. In *Neural Information Processing Systems (NeurIPS)*, 2018.
- Singh, G., Gehr, T., Püschel, M., and Vechev, M. T. An abstract domain for certifying neural networks. *Proc. ACM Program. Lang.*, 3(POPL), 2019.
- Szegedy, C., Zaremba, W., Sutskever, I., Bruna, J., Erhan, D., Goodfellow, I. J., and Fergus, R. Intriguing properties of neural networks. In *Proc. of International Conference on Learning Representations (ICLR)*, 2014.
- Tjeng, V., Xiao, K. Y., and Tedrake, R. Evaluating robustness of neural networks with mixed integer programming. In *Proc. of International Conference on Learning Representations (ICLR)*, 2019.
- Tramèr, F., Carlini, N., Brendel, W., and Madry, A. On adaptive attacks to adversarial example defenses. In *Neural Information Processing Systems (NeurIPS)*, 2020.
- Wang, S., Zhang, H., Xu, K., Lin, X., Jana, S., Hsieh, C., and Kolter, J. Z. Beta-crown: Efficient bound propagation with per-neuron split constraints for neural network robustness verification. In *Neural Information Processing Systems (NeurIPS)*, 2021.
- Wong, E. and Kolter, J. Z. Provable defenses against adversarial examples via the convex outer adversarial polytope. In *Proc. of International Conference on Machine Learning (ICML)*, volume 80, 2018.
- Wong, E., Schmidt, F. R., Metzen, J. H., and Kolter, J. Z. Scaling provable adversarial defenses. In *Neural Information Processing Systems (NeurIPS)*, 2018.
- Xu, K., Shi, Z., Zhang, H., Wang, Y., Chang, K., Huang, M., Kaillkhura, B., Lin, X., and Hsieh, C. Automatic perturbation analysis for scalable certified robustness and beyond. In *Neural Information Processing Systems (NeurIPS)*, 2020.
- Zhang, B., Cai, T., Lu, Z., He, D., and Wang, L. Towards certifying l-infinity robustness using neural networks with l-inf-dist neurons. In *Proc. of International Conference on Machine Learning (ICML)*, volume 139, 2021.
- Zhang, B., Jiang, D., He, D., and Wang, L. Boosting the certified robustness of l-infinity distance nets. In *Proc. of International Conference on Learning Representations (ICLR)*, 2022a.
- Zhang, B., Jiang, D., He, D., and Wang, L. Rethinking lipschitz neural networks and certified robustness: A boolean function perspective. *CoRR*, abs/2210.01787, 2022b. doi: 10.48550/arXiv.2210.01787.
- Zhang, H., Weng, T., Chen, P., Hsieh, C., and Daniel, L. Efficient neural network robustness certification with general activation functions. In *Neural Information Processing Systems (NeurIPS)*, 2018.
- Zhang, H., Chen, H., Xiao, C., Goyal, S., Stanforth, R., Li, B., Boning, D. S., and Hsieh, C. Towards stable and efficient training of verifiably robust neural networks. In *Proc. of International Conference on Learning Representations (ICLR)*, 2020.
- Zhang, H., Wang, S., Xu, K., Li, L., Li, B., Jana, S., Hsieh, C., and Kolter, J. Z. General cutting planes for bound-propagation-based neural network verification. *ArXiv preprint*, abs/2208.05740, 2022c.

## A. Averaging Multipliers Makes Gradients Efficient

**Theorem 1.** Let  $x_i$  be i.i.d. drawn from the dataset and define  $f_i = f_\theta(x_i)$  and  $g_i = g_\theta(x_i)$ , where  $f_\theta$  and  $g_\theta$  are two functions. Further, define  $L_1 = (\sum_{i=1}^n \frac{1}{n} f_i) \cdot (\sum_{i=1}^n \frac{1}{n} g_i)$  and  $L_2 = \sum_{i=1}^n \frac{1}{n} f_i g_i$ . Then, assuming the function value and the gradient are independent,  $\mathbb{E}_x(\frac{\partial L_1}{\partial \theta}) = \mathbb{E}_x(\frac{\partial L_2}{\partial \theta})$  and  $\text{Var}_x(\frac{\partial L_1}{\partial \theta}) \leq \text{Var}_x(\frac{\partial L_2}{\partial \theta})$ .

*Proof.* A famous result in stochastic optimization is that stochastic gradients are unbiased. For completeness, we give a short proof of this property: Let  $L = \mathbb{E}_x f(x) = \int_{-\infty}^{+\infty} f(x) dP(x)$ , thus  $\nabla_x L = \nabla_x (\int_{-\infty}^{+\infty} f(x) dP(x)) = \int_{-\infty}^{+\infty} \nabla_x f(x) dP(x) = \mathbb{E}_x(\nabla_x f(x))$ . Therefore,  $\nabla f(x_i)$  is an unbiased estimator of the true gradient.

Applying that the stochastic gradients are unbiased, we can write  $\nabla_\theta f_i = \nabla_\theta f + \eta_i$ , where  $\nabla_\theta f$  is the expectation of the gradient and  $\eta_i$  is the deviation such that  $\mathbb{E}\eta_i = 0$  and  $\text{Var}(\eta_i) = \sigma_1^2$ . Since  $x_i$  is drawn independently,  $f_i$  are independent and thus  $\eta_i$  are independent. Similarly, we can write  $\nabla_\theta g_i = \nabla_\theta g + \delta_i$ , where  $\mathbb{E}\delta_i = 0$  and  $\text{Var}(\delta_i) = \sigma_2^2$ .  $\eta_i$  and  $\delta_i$  may be dependent.

Define  $\bar{f} = \sum_i \frac{1}{n} f_i$  and  $\bar{g} = \sum_i \frac{1}{n} g_i$ . Explicit computation gives us that  $\nabla L_1 = \bar{g} (\sum_i \frac{1}{n} \nabla f_i) + \bar{f} (\sum_i \frac{1}{n} \nabla g_i)$ , and  $\nabla L_2 = \sum_i \frac{1}{n} (f_i \nabla g_i + g_i \nabla f_i)$ . Therefore,

$$\mathbb{E}_x(\nabla_\theta L_1 | f_i, g_i) = \bar{g} \nabla_\theta f + \bar{f} \nabla_\theta g = \mathbb{E}_x(\nabla_\theta L_2 | f_i, g_i).$$

By the law of total probability,

$$\begin{aligned} \mathbb{E}_x(\nabla_\theta L_1) &= \mathbb{E}_{f_i, g_i}(\mathbb{E}_x(\nabla_\theta L_1 | f_i, g_i)) \\ &= \mathbb{E}_{f_i, g_i}(\mathbb{E}_x(\nabla_\theta L_2 | f_i, g_i)) \\ &= \mathbb{E}_x(\nabla_\theta L_2). \end{aligned}$$

Therefore, we have got the first result: the gradients of  $L_1$  and  $L_2$  have the same expectation.

To prove the variance inequality, we will use variance decomposition formula<sup>3</sup>:

$$\begin{aligned} \text{Var}_x(\nabla_\theta L_k) &= \mathbb{E}_{f_i, g_i}(\text{Var}_x(\nabla_\theta L_k | f_i, g_i)) + \\ &\quad \text{Var}_{f_i, g_i}(\mathbb{E}_x(\nabla_\theta L_k | f_i, g_i)), \end{aligned}$$

$k = 1, 2$ . We have proved that  $\mathbb{E}_x(\nabla_\theta L_1 | f_i, g_i) = \mathbb{E}_x(\nabla_\theta L_2 | f_i, g_i)$ , thus the second term is equal. Next, we prove that  $\text{Var}_x(\nabla_\theta L_1 | f_i, g_i) \leq \text{Var}_x(\nabla_\theta L_2 | f_i, g_i)$ , which implies  $\text{Var}_x(\nabla_\theta L_1) \leq \text{Var}_x(\nabla_\theta L_2)$ .

By explicit computation, we have

$$\begin{aligned} \text{Var}(\nabla L_1 | f_i, g_i) &= (\bar{g})^2 \text{Var}\left(\sum_i \frac{1}{n} \eta_i\right) + (\bar{f})^2 \text{Var}\left(\sum_i \frac{1}{n} \delta_i\right) \\ &= \frac{1}{n} \sigma_1^2 (\bar{g})^2 + \frac{1}{n} \sigma_2^2 (\bar{f})^2, \end{aligned} \quad (5)$$

and

$$\begin{aligned} \text{Var}(\nabla L_2 | f_i, g_i) &= \text{Var}\left(\sum_i \frac{1}{n} f_i \delta_i\right) + \text{Var}\left(\sum_i \frac{1}{n} g_i \eta_i\right) \\ &= \frac{1}{n} \sigma_1^2 \left(\sum_i \frac{1}{n} g_i^2\right) + \frac{1}{n} \sigma_2^2 \left(\sum_i \frac{1}{n} f_i^2\right). \end{aligned} \quad (6)$$

Applying Jensen's formula on the convex function  $x^2$ , we have  $(\sum_i \frac{1}{n} a_i)^2 \leq \sum_i \frac{1}{n} a_i^2$  for any  $a_i$ , thus  $(\bar{f})^2 \leq \sum_i \frac{1}{n} f_i^2$  and  $(\bar{g})^2 \leq \sum_i \frac{1}{n} g_i^2$ . Combining Equation (5) and Equation (6) with these two inequalities gives the desired result.  $\square$

## B. Experiment Details

### Algorithm 1 Train Loss Computation

---

**Input:** data  $X_B = \{(\mathbf{x}_b, y_b)\}_b$ , current  $\epsilon$ , target  $\epsilon^t$ , network  $\mathbf{f}$   
**Output:** A differentiable loss  $L$   
 $\mathcal{L}_{\text{IBP}} = \sum_{b \in \mathcal{B}} \mathcal{L}_{\text{IBP}}(\mathbf{x}_b, y_b, \epsilon) / |\mathcal{B}|$ .  
**if**  $\epsilon < \epsilon^t$  **then**  
     //  $\epsilon$  annealing regularisation from Shi et al. (2021)  
      $\mathcal{L}_{\text{fast}} = \lambda \cdot (\mathcal{L}_{\text{tightness}} + \mathcal{L}_{\text{relu}})$   
     **return**  $\mathcal{L}_{\text{IBP}} + \epsilon / \epsilon^t \cdot \mathcal{L}_{\text{fast}}$   
**end if**  
 $\mathcal{L}_{\text{TAPS}} = \sum_{b \in \mathcal{B}} L_{\text{TAPS}}(\mathbf{x}_b, y_b, \epsilon) / |\mathcal{B}|$ .  
**return**  $\mathcal{L}_{\text{IBP}} \cdot \mathcal{L}_{\text{TAPS}}$

---

### B.1. TAPS Training Procedure

To obtain state-of-the-art performance with IBP, various training techniques have been developed. We use two of them:  $\epsilon$  annealing (Gowal et al., 2018) and initialization and regularization for stable box sizes (Shi et al., 2021).  $\epsilon$  annealing slowly increases the perturbation magnitude  $\epsilon$  during training to avoid exploding approximation sizes and thus gradients. The initialization of Shi et al. (2021) scales network weights to achieve constant box sizes over network depth and their regularization  $\mathcal{L}_{\text{fast}}$  controls ReLU activation states during the  $\epsilon$  annealing phase. During the  $\epsilon$  annealing phase, we combine the IBP loss with the ReLU stability regularization  $\mathcal{L}_{\text{fast}}$ , before switching to the TAPS loss as described in Section 3.4. We formalize this in Algorithm 1.

<sup>3</sup>[https://en.wikipedia.org/wiki/Law\\_of\\_total\\_variance](https://en.wikipedia.org/wiki/Law_of_total_variance)

Table 5: The training epoch and learning rate settings.

Dataset	Batch size	Total epochs	Annealing epochs	Decay-1	Decay-2
MNIST	256	70	20	50	60
CIFAR-10	128	160	80	120	140
TinyImageNet	128	80	20	60	70

 Table 6: The  $L_1$  coefficient, training and certification time cost for the best classifier splits for TAPS.

	$\epsilon$	# ReLUs in Classifier	$L_1$	Train Time [s]	Certify Time [s]
MNIST	0.1	3	1e-6	42622	17117
	0.3	1	0	12417	41624
CIFAR-10	2/255	5	2e-6	141281	166474
	8/255	1	2e-6	27017	26968
TinyImageNet	1/255	1	0	306036	23497

## B.2. Data Augmentation

The data preprocessing mostly follows Müller et al. (2022a). For MNIST, we do not apply any preprocessing. For CIFAR-10 and TinyImageNet, we normalize with the dataset mean and standard deviation (after calculating perturbation size) and augment with random horizontal flips. For CIFAR-10, we apply random cropping to  $32 \times 32$  after applying a 2 pixel padding at every margin. For TINYIMAGENET, we apply random cropping to  $56 \times 56$  during training and center cropping during testing.

## B.3. Model Architectures

Unless specified otherwise, we follow Shi et al. (2021); Müller et al. (2022a) and use a CNN7 with Batch Norm for our main experiments. CNN7 is a convolutional network with 7 convolutional and linear layers. All but the last linear layer are followed by a Batch Norm and ReLU layer.

## B.4. Training Details

We follow the hyperparameter choices of Shi et al. (2021) for  $\epsilon$ -annealing, learning rate schedules, batch sizes, and gradient clipping (see Table 5). We set the initial learning rate to 0.0005 and decrease it by a factor of 0.2 at Decay-1 and -2. We set the gradient clipping threshold to 10.

We use additional  $L_1$  regularization in some settings where we observe signs of overfitting. We report the  $L_1$  regularization and split position chosen for different settings in Table 6.

We train using single NVIDIA GeForce RTX 3090 for MNIST and CIFAR-10 and single NVIDIA TITAN RTX for TINYIMAGENET.

## B.5. Certification Details

We combine IBP (Gowal et al., 2018), CROWN-IBP (Zhang et al., 2020), and MN-BAB (Ferrari et al., 2022) for certification running the most precise but also compu-

Table 7: Comparison of TAPS accuracy with certified and adversarial accuracy.

Dataset	cor(TAPS, cert.)	cor(TAPS, adv.)	TAPS – cert.	TAPS – adv.
MNIST	0.9139	0.9633	$0.0122 \pm 0.0141$	$0.0033 \pm 0.0079$
CIFAR-10	0.9973	0.9989	$0.0028 \pm 0.0095$	$-0.0040 \pm 0.0077$

tationally costly MN-BAB only on samples not certified by the other methods. We use the same configuration for MN-BAB as Müller et al. (2022a). The certification is run on a single NVIDIA TITAN RTX.

We use a mixture of strong adversarial attacks to evaluate adversarial accuracy. First, we run PGD attacks with 5 restarts and 200 iterations each. Then, we run MN-BaB to search for adversarial examples with a timeout of 1000 seconds.

## C. Extended Evaluation

**TAPS Accuracy as GoF** In practice, we want to avoid certifying every model with expensive certification methods, especially during hyperparameter tuning and applying early stopping. Therefore, we need a criterion to select models. In this section, we aim to show that TAPS accuracy is a good instrument for goodness of fit (GoF).

We compare the TAPS accuracy to adversarial and certified accuracy with all models we get on MNIST and CIFAR-10. The result is shown in Table 7. From Table 7, we can see that the correlations between TAPS accuracy and both the adversarial and the certified accuracy are close to 1. In addition, the differences are small and centered at zero, with a small standard deviation. Therefore, we conclude that TAPS accuracy is a good estimate of the true robustness, thus a good measurement of GoF. In all the experiments, we perform model selection based on the TAPS accuracy.

**Training Difficulty** Since TAPS is merely a training technique, we can test TAPS-trained models trained with a new classifier split. By design, if the training is successful, then under a given classifier split for testing, the model trained with the same split should have the best TAPS accuracy. Although this is often true, we find that in some cases, a smaller classifier split results in higher TAPS accuracy, indicating the difficulty of training.

Figure 8 shows the tested TAPS accuracy for models trained with IBP and different splits for CIFAR-10. The result on MNIST is provided in Figure 9. From these figures, we can see that for CIFAR-10  $\epsilon = 2/255$  and MNIST, the models trained with the same test split has the highest TAPS accuracy, as expected. However, for CIFAR-10  $\epsilon = 8/255$ , the model trained with classifier size 4 is consistently better for all test splits. Furthermore, as we show in Section 4.3, this model has the best adversarial and certified accuracy as

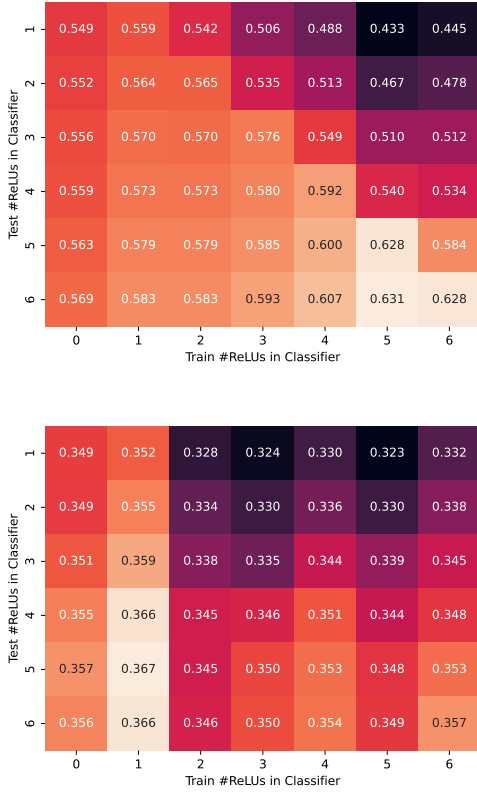


Figure 8: TAPS accuracy of models trained by different classifier size. The top subfigure is on CIFAR-10  $\epsilon = \frac{2}{255}$ ; the bottom subfigure is on CIFAR-10  $\epsilon = \frac{8}{255}$ .

well. This means that in this setting, the training of larger splits is too difficult, such that TAPS is not able to find a good model to minimize the given loss. However, in other settings, TAPS is easy enough to train.

**Split Position** We include the full tables of the experiment in Section 4.3 in Table 8 and Table 9.

Table 8: Effect of split position into the classifier and feature extractor (overall model size remains unchanged). All numbers are in percentages. All results for MNIST.

$\epsilon$	# ReLUs in Classifier	Nat.	Adv.	Cert.			
				Total	IBP	C-IBP	MN-BaB
0.1	0	98.87	98.16	98.13	97.83	+0.17	+0.13
	1	99.06	98.37	98.31	96.27	+1.52	+0.52
	2	99.16	98.35	98.25	87.82	+8.11	+2.32
	3	99.19	<b>98.51</b>	<b>98.39</b>	62.83	+27.34	+8.22
	4	<b>99.28</b>	98.47	98.03	4.75	+47.25	+46.03
	5	99.22	<b>98.51</b>	98.17	9.76	+53.32	+35.09
	6	99.09	98.45	98.27	81.89	+12.62	+3.76
0.3	0	97.60	93.37	93.15	93.08	+0.03	+0.04
	1	97.94	94.01	<b>93.62</b>	92.76	+0.55	+0.31
	2	98.16	94.18	93.55	91.85	+0.87	+0.83
	3	98.63	94.48	93.03	89.40	+1.60	+2.03
	4	98.7	94.85	93.44	89.52	+1.83	+2.09
	5	98.63	94.64	93.26	89.15	+1.98	+2.13
	6	<b>98.88</b>	<b>95.11</b>	92.70	85.03	+3.61	+4.06

Table 9: Effect of split position into the classifier and feature extractor (overall model size remains unchanged). All numbers are in percentages. All results for CIFAR-10.

$\epsilon$	#ReLUs in Classifier	Nat.	Adv.	Cert.		
				Total	IBP	MN-BaB
2/255	0	67.27	56.32	56.14	53.54	+2.60
	1	70.10	57.78	57.48	41.86	+15.62
	2	70.74	57.83	57.39	40.24	+17.25
	3	71.88	58.89	58.23	34.41	+23.82
	4	72.45	60.38	59.47	31.88	+27.59
	5	75.09	<b>63.00</b>	<b>61.56</b>	24.36	+37.20
	6	<b>75.40</b>	62.73	61.11	24.90	+36.21
8/255	0	48.15	34.63	34.60	34.26	+0.34
	1	49.76	<b>35.29</b>	<b>35.10</b>	32.92	+2.18
	2	47.28	33.54	33.12	28.94	+4.18
	3	48.76	33.50	33.12	29.14	+3.98
	4	50.19	34.78	34.35	29.14	+5.21
	5	50.2	34.33	33.72	28.83	+4.89
	6	<b>51.03</b>	35.25	34.44	29.97	+4.47



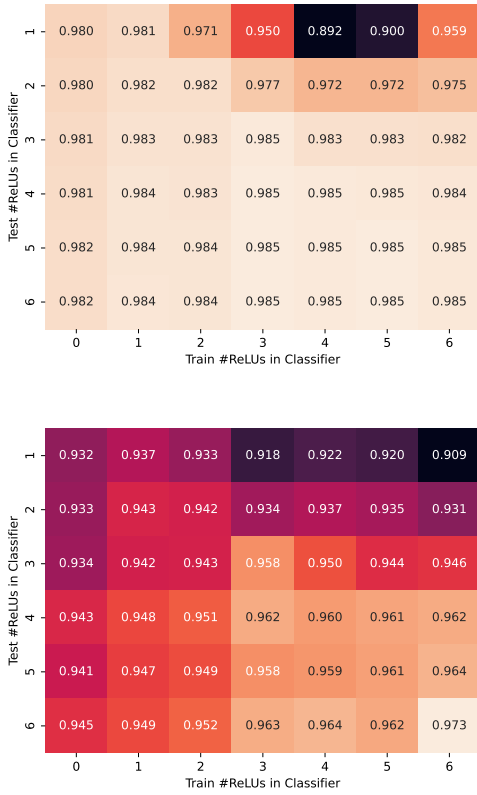


Figure 9: TAPS accuracy of models trained by different classifier size. The top subfigure is on MNIST  $\epsilon = 0.1$ ; the bottom subfigure is on MNIST  $\epsilon = 0.3$ .